$LiNbO_3$ films - a low-cost alternative lead-free piezoelectric material for vibrational energy harvesters

Giacomo Clementi[1*], Giulia Lombardi[2], Samuel Margueron[1], Miguel Angel Suarez[1], Eric Lebrasseur[1], Sylvain Ballandras[3], Joel Imbaud[1], Franck Lardet-Vieudrin[1], Ludovic Gauthier-Manuel[1], Bernard Dulmet[1], Mickael Lallart[2], and Ausrine Bartasyte[1]

[1] *FEMTO-ST Institute, University of Bourgogne Franche-Comté, CNRS (UMR 6174), ENSMM, 26 rue de l'Epitaphe, 25030 Besançon, France*

[2] *Univ. Lyon, INSA-Lyon, LGEF EA 682, F-69621, France*

[3] *frec|n|sys SAS, 18 Rue Alain Savary, 25000 Besançon, France*

[*] *Corresponding author: giacomo.clementi@femto-st.fr*

Lead-free lithium niobate ($LiNbO_3$) piezoelectric transducer is considered as a substitute to lead-based solutions for vibrational energy scavenging applications. Taking into account the much lower dielectric constant of $LiNbO_3$ crystal compared to conventional piezoceramics (for instance PZT), we implement, in a global optimization approach, a thick single crystal film on silicon substrate with optimized clamped capacitance for better impedance–matching conditions. We design a piezoelectric cantilever based on (YX*l*)/36° $LiNbO_3$ cut, enhancing the output voltage to achieve piezoelectric transducer performance compatible with harvesting device standards. For a cantilever with bending first resonant frequency of 1.14 kHz, an output power up to 380 µW is achieved, yielding a power density of 8.26 $\mu W.mm^{-2}$, therefore comparable to lead–based and –free piezoelectric harvesters, while featuring a widely used material with well-established production process (hence lowering the cost for instance). The harvesting capabilities of the device allows starting a sensor node (from zero energy initial conditions) after 9 seconds only and then maintaining the possibility of sending data every 2 seconds (each transmission event consuming approximately 420 µJ) under continuous excitation.

1. Introduction

In recent years, a strong research effort has been devoted to harvest the energy available in the environment and use it as an electrical power source to power IoT (Internet of Things) applications. Some examples include wheel sensors, structural health monitoring, wearable and portable healthcare devices, distributed wireless sensor networks in smart agriculture, home and industry smart automation, and everywhere where reliable and long-lasting primary electrical energy source (*i.e.*, conventional batteries) cannot be used (for example due to difficult access or harsh environment). Energy harvesting (EH) from vibrations has become a focus of interest during the past decades in line with the advent of very low (< 100 µW) power and portable electronics. Over the last decade, miniaturization of harvesters using MEMS technology with piezoelectric films or nano-composites came into the focus of interest in

order to harvest energy from vibrations and to power small systems such as wireless nodes and sensors [1,2]. Hence, a particular interest has been placed on the possibility of integrating the transducer with the electronic part on the same wafer.

At present, many different ferroelectric ($PbZr_{1-x}Ti_xO_3$ (PZT), $BaTiO_3$ (BTO), $K_{1-x}Na_xNbO_3$ (KNN), etc.) and non-ferroelectric (AlN, ZnO, etc.) piezoelectric materials in the form of films, nanostructures and ceramic/crystals bonded on wafers are explored for the fabrication of Piezoelectric Vibration Energy Harvesters (PiViEHs). Obtaining high power output from piezoelectric harvesters in many applications requires a significant electromechanical coupling, *k*; this resulted in the preference and common use of bulk PZT in piezoelectric harvesters. Recently, it was demonstrated that it was possible to generate an output power of 1.2 mW (at resonance of 250 Hz from a base excitation) vibration sources by using six advanced 5 x 5 cm^2 PZT bimorph beams [3]. Nevertheless, the large scale of global deployment for IoT applications requires to consider the piezoelectric material grey energy, abundance, recyclability and toxicity (ROHS compliance, REACH regulation). Therefore, in future, PZT has to be replaced by lead-free materials [4], whatever its form and shape. Non-ferroelectric piezoelectric materials such as ZnO and AlN and their derivatives, have much lower *k* factor than PZT (by one order of magnitude, typically), but offer compatibility with conventional integrated circuit technology fabrication process. Recently, it was shown that the transverse piezoelectric coefficient and the figure of merit of the well-known piezoelectric film material AlN (001) increase considerably by partially substituting Al by Sc [5,6]. Further effort is done to increase Sc concentration within the films to achieve electromechanical coupling coefficients similar to that of PZT. One of the highest power density values (1.6 $mW.cm^{-3}$) among the micro-PiViEHs with wide bandwidth of 253 Hz was achieved by EH based on lead-free KNN films [7]. However, synthesis of KNN films is still far from being a routine due to difficulty to control alkaline oxide composition [8], preventing their commercial application as energy harvesters which remains a niche market.

On the other hand, lithium niobate ($LiNbO_3$) crystal is an industrially produced piezoelectric material easily accessible, rare-earth and toxic-element-free, cheap, available in form of wafers (with diameter up to 6 inches), widely exploited for developments of acoustics and optical devices [9], and presenting similar efficiency in energy harvesting as commonly used $PbZr_{1-x}Ti_xO_3$ (PZT) [4]. The major advantages of $LiNbO_3$ over PZT are: (i) extremely chemically inert material; (ii) very high Curie temperature (> 1150 °C) thus compatible with EH at high temperatures (PZT limit < 150 °C). However, the $LiNbO_3$ applications in acoustics are limited to 300 °C by the increased losses at high temperatures due to ionic conductivity. It is important to note that the requirements in terms of losses are much lower in the case of energy harvesting applications. Although the implementation of $LiNbO_3$ crystals as high-temperature transducers (up to 1000 °C [10]) and preliminary investigations as energy harvesters (at least up to 500 °C [11]) were demonstrated, further studies are needed to confirm the suitability of $LiNbO_3$ for high-temperature applications in actuators and energy harvesters, especially when considering application-oriented designs. The piezoelectric energy harvesting demonstration was

investigated so far by using industrially available $LiNbO_3$ wafers with thickness of 500 ÷ 1000 μm [12,13,14]. However, $LiNbO_3$ presents dielectric constant much lower than those of piezoelectric ceramics (unconstrained $\varepsilon^T_{33}/\varepsilon_0 = 28.85$ and $\varepsilon^T_{11}/\varepsilon_0 = 84.45$ [15]). In the case of micro-energy harvesters where lateral dimensions are limited, such thick wafers cannot be used due to issues in impedance–matching with EH circuits as well as structural compatibility with the substrate. Moreover, bulk $LiNbO_3$ crystals are very brittle and only low displacement can be attained. Therefore, $LiNbO_3$ film technology has to be implemented in vibrational energy harvesting to overcome such issues and provide realistic operations. Despite their promising properties, the application of $LiNbO_3$ films in piezoelectric vibrational energy harvesting is still very little studied and considerable efforts have to be done towards their integration in the conventional processing of MEMS and EH devices.

In this paper, we experimentally demonstrate a suitable microfabrication process and the successful application of vibrational energy harvesters based on thick (10 to 30 μm) single-crystal $LiNbO_3$ films bonded on Si substrates. The capacitance, electromechanical coupling and power density were studied analytically and designed with respect to the target application, while resonant frequencies, voltage and displacement response of studied structures were simulated by Finite Element Method. Hence, the potentials of $LiNbO_3$ piezoelectric films for EH are confirmed, showing comparable and even higher power densities than conventional Pb-based and Pb-free energy harvesters.

2. Theoretical Considerations

$LiNbO_3$ belongs to *3m* point group, showing three plane–mirror symmetry. Moreover, it is also a part of the space group *R3c*, where crystals show threefold rotation along *c*-axis, or [0001] direction. To investigate the material properties of $LiNbO_3$, we started from a reference system where the crystallographic *c*-axis is parallel to *Z*-axis in the standard orthogonal direction. Then, to model a specific orientation cut for $LiNbO_3$, we have to consider a plate where the *X*-axis is parallel to *a*-axis, and the perpendicular *Y*-axis is in the same plane. In this configuration we can improve the electromechanical coupling of the material starting from a standard 90° (YXl) or ZX plate (orientation defined according IEEE Std-176 convention [16]). To model the piezoelectric element orientation, we used the matrix notation where $i, j = 1,2,3$ are defined as in Fig. 1a. In order to increase the piezoelectric response, we considered the rotated piezoelectric tensor for a beam that was oriented along the rotated *Z'*-axis of $LiNbO_3$, while the electrical displacement of the charges was rotated along the *Y'*-axis. The orientation study is implemented using a rotation around *X*-axis for a given angle parameter ψ. An example of $LiNbO_3$ piezoelectric tensor anisotropy is represented in 3D tensor form for the specific orientation (YXl)/36° (Fig. 1b) that is considered in the present study. In this representation, we can see both positive and negative piezoelectric coefficient values (absolute value is ranging from 0 to 38 pC/N) of the tensor when a rotation is performed with $\psi = 36°$. The obtained properties for this given single crystal orientation will be discussed in the simulation section in comparison with PZT-5A and other

selected Pb-free materials. Before introducing the concept of electromechanical coupling, we shall use the following set of two equations for investigating the direct and converse piezoelectric effect:

$$\begin{cases} S = s^E T + d^t E \\ D = dT + \varepsilon^T E \end{cases} \quad (1)$$

where S is the strain, T the stress, d the piezoelectric coefficient, s^E the elastic compliance at constant electric field, ε is the permittivity at constant stress, E the electric field, and D the dielectric displacement. When the cantilever undergoes bending deformation, the strain on the piezoelectric element gives an orthogonal displacement of charges; this configuration of the harvester is called transverse mode. For a given piezoelectric material, we define the material electromechanical coupling coefficient k, as the ratio between stored electrical energy and input mechanical energy, which is generally expressed as:

$$k_{ij} = \sqrt{\frac{d_{ij}^2}{s_{jj}^E \varepsilon_{ii}^T}} \quad (2)$$

Here, we assumed the most common transverse mode configuration. For the case of ceramics, we would consider k_{31}, where '*3*' indicates the polarization direction, and '*1*' the deformation direction, where d_{31} is the piezoelectric coefficient, s_{11} the compliance and ε_{33} the permittivity for the given configuration. Two important figures of merit for piezoelectric materials are the one discussed in detail in [17,18]. These are defined respectively for stress-driven (FoM^T) and strain-driven (FoM^S) piezoelectric generators. The former is defined as:

$$FoM^T = \frac{d_{ij}^2}{\varepsilon_{ii}^T} \quad (3)$$

which for a constant stress load does not depend on the compliance of the piezoelectric material. Differently, in the case of strain-driven harvesters, it is necessary to take into account the fact that most of the times, the transducers do not work in open circuit conditions, therefore we have to consider the compliance in short circuit condition, finally FoM^S is defined as:

$$FoM^S = \frac{d_{ij}^2}{s_{jj}^E s_{jj}^D \varepsilon_{ii}^T} \quad (4)$$

Where s_{jj}^D is the compliance at constant electric displacement field. These two figures of merit are showing how for different excitation types, it is possible to maximize the output electrical energy and are useful to make a comparison between different materials. In general, it is clear that in both cases a high value of k_{ij} is required in order to design an efficient harvester.

When considering a high-level analysis of the system, the piezoelectric device can be modeled as a single degree of freedom oscillator resonating near one of its resonance frequencies. Consequently, the structure can be modeled as a spring-mass-damper system dynamically excited by an external force (or equivalently an acceleration), and generating a voltage V from the deformation displacement u. The system can then be described by the following set of dynamic equations:

$$\begin{cases} F = M\ddot{u} + C\dot{u} + K_E u + \alpha V \\ I = \alpha\dot{u} - C_0\dot{V} \end{cases} \quad (5)$$

where F is the external force, K_E the open-circuit stiffness of the system, M the dynamic mass, α is the electromechanical force factor, I the current, C the viscous damping and C_0 the clamped capacitance. The electromechanical equivalent circuit for the piezoelectric transducer is presented in Fig. 2, in which the coupling term is represented by a transformer. The external force applied on the mechanical branch of the circuit generates a base velocity $\dot{u}$ that is equivalent to a current in the electrical model, then the transformer with α ratio is converting the mechanical velocity into current in the electrical branch of the circuit. In this approximation, we can calculate the electromechanical coupling factor for the structure, k_{eff}^2 defined as:

$$k_{eff}^2 = \frac{\alpha^2}{C_0 K_E + \alpha^2} \quad (6)$$

which represents the effective coupling of the structure during the energy conversion process. Furthermore, the quality factor of the structure can be found as:

$$Q = \sqrt{\frac{MK_E}{C}} \quad (7)$$

In this paper, we will discuss how to tailor the material electro-mechanical coupling factor in order to have realistic impedance–matching between the piezoelectric transducer and the electronic interface, while for the structural coupling we will present the value measured for our given device. Typically, the output voltage from our piezoelectric generator will be sinusoidal, whereas in order to power a sensor node, as per our application, a DC voltage supply is needed. Hence, the rectification circuit designed for our prototype is a half-bridge rectifier (Fig. 3). In this configuration we used two diodes and two smoothing capacitors C_r connected to an equivalent resistive load R_l. This interface can rectify and double the voltage amplitude degraded by the threshold voltage of the diodes. Eventually, V_{DC} generated at resonance frequency f_0, can be expressed as a function of the displacement magnitude u_M as:

$$V_{DC} = \frac{2\alpha\, f_0 R_l}{f_0 R_l C_0 + 1} u_M \quad (8)$$

The harvested power from the rectified V_{DC} voltage, is simply $P = \frac{V_{DC}^2}{R_l}$, giving the following equation:

$$P = \frac{4\alpha^2 f_0^2 R_l}{(f_0 R_l C_0 + 1)^2} u_M^2 \quad (9)$$

In the experimental section, more details will be given regarding the electronic interface, along with a comparison between the theoretical and experimental harvested power.

3. Material and Methods

A commercial 500 µm thick (YXl)/36° $LiNbO_3$ wafer (from Roditi) was used to fabricate thick film on Si substrate (Fig. 4). 200 nm thick Au layers with Cr adhesive layers, were deposited on one side of the $LiNbO_3$ wafer and on one side of a 500 µm thick Si wafer. The Si wafer presented thermal oxide with thickness of 0.5 µm. Then, the $LiNbO_3$ and Si wafers were bonded by means of mechanical compression of Au layers (EVG wafer bonder [19]). The $LiNbO_3$ wafer was subsequently thinned by lapping steps to an overall thickness of 32 µm, which was followed by a micro-polishing step. Then, the Si wafer was polished down to 360 µm thickness. Aluminum electrodes with thickness of 300 nm were structured on the $LiNbO_3$ surface by lift-off process using UV lithography and evaporation deposition technique. The cantilevers were diced mechanically from (32 µm)$LiNbO_3$/(400 nm)Au-Cr/(1 µm)SiO_2/(360 µm)Si structure by means of a dicing saw. The final dimensions of the cantilevers, without considering the clamping, were 20 mm in length and 5 mm in width. The electrode was partially covering the structure, resulting in an active surface of 46 mm^2. The Cr/Au layer used for wafer bonding was also acting as bottom electrode of the device. We show on Fig. 4(e) the cross-section of the cantilever. The photograph was taken with optical microscope from a lateral side, we could clearly see the Cr/Au bottom electrode, while the upper layer was $LiNbO_3$, and the bottom one the Si/SiO_2 substrate. Finally, Fig. 4(f) presents the cantilever after dicing.

4. Simulations

To achieve some predictive results concerning the voltage output and the displacement response of our system, finite element modeling (FEM) was carried out with COMSOL Multiphysics software in different dynamic conditions. We modeled the structure in 3D as a unimorph bender with silicon substrate and $LiNbO_3$ as piezoelectric element. Euler angles were used to implement the oriented cut. Resonant frequency, vibrational modes and material properties were simulated thereafter by FEM.

In particular, the material properties of (YXl)/36° $LiNbO_3$ cut, were simulated with both FEM software and analytical model. The values obtained for a rotation of 36° around X-axis were 65.3 for relative unconstrained permittivity ε_r^*, and -18.1 pC/N as effective piezoelectric coefficient d_{23}^* [20]. The results on the piezoelectric coupling factor from static FEM analysis gave the same conclusion as the analytical model. Although the transverse piezoelectric coefficient of (YXl)/36° $LiNbO_3$ orientation is lower by one order of magnitude than that of PZT-5A (d_{31} = -171 pC/N [21]), its lower relative permittivity compared to that of PZT-5A (1700-1800 [22]) yields similar electromechanical coupling coefficient in this orientation ($k_{31}^{\text{PZT-5A}} = 34\ \%$, $k_{23}^{\text{LiNbO}_3} = 32\ \%$), making it a suitable alternative for energy harvesting applications. A comparison between the two coupling factors k_{ij} and FoMs is presented in Table 1. All the materials in the table are bulk materials [23,24,25], and we estimated the value of s_{jj}^{D} using the

relation $s_{jj}^{D} = s_{jj}^{E}(1- k_{ij}^{2})$, in this way we can compare easily both electromechanical coupling and figure of merit. For stress-driven harvesters, (YXl)/36° $LiNbO_3$ shows comparable FoM^T with Pb-free materials and can be further improved by the choice of more suitable crystal cut. On the contrary, for strain-driven harvesters, (YXl)/36° $LiNbO_3$ has the highest figure of merit, achieving the theoretical value of 19.5 $kJ.cm^{-3}$.

For dynamic modeling, we used the same 3D model and proceeded to simulate the voltage response and displacement of the structure, based on the proposed design. The investigations were done at different acceleration levels in order to have a reference and to countercheck the cantilever response and the expected results. In Fig. 5 are shown the results of the simulations, with the acceleration levels were ranging from 0.1 g to 3.6 g. The study was performed in the frequency domain, considering the bending resonance frequency of 1.163 kHz, and studying the displacement and voltage response in open circuit conditions. The peak displacement, taking as a reference the free–end edge of the cantilever, is plotted for each considered acceleration. The low entity of the tip displacement is the result of the silicon substrate stiffness, which was modeled considering Si (100) orientation. We acknowledged that the displacement was measured approximately around the free end of the cantilever, so that the simulated value reached a maximum of 26.4 µm. On the right-hand side of the figure, the voltage response is presented. In this case, considering the piezoelectric coupling given by (YX*l*)/36° $LiNbO_3$ orientation, the peak voltage simulated is reaching a maximum of 23.9 V. Also, at lower acceleration levels (1 g), the voltage response is in a useful range of values, with the peak voltage around 6.4 V. The results are given using the isotropic loss–factor approximation for the structure. As we expected for a simple cantilever, both displacement and voltage are evolving linearly when increasing the acceleration levels. The 3D insets in the graph of Fig. 5 are representing the response at the simulated resonance frequency for the structure at 3.4 g, in order to compare with the experimental results.

5. Experimental Results and Discussion

During tests, the piezoelectric beam was clamped on a 3D-printed sample holder, while the top and bottom electrodes were put on a PCB board for the connection to the energy extraction circuit as well as monitoring the voltage output. The samples were characterized with a HP4194A network analyzer in order to investigate the capacitance and electromechanical coupling of the fabricated cantilevers. The structural electromechanical coupling factor, k_{eff}^{2}, and the quality factor, Q, were estimated from measured resonance and anti-resonance frequencies [16]. The dynamic characterization of voltage response and displacement was carried out separately. The associated experimental setup was composed of a shaker providing a base excitation, controlled by a waveform generator and a power amplifier. An oscilloscope was used for monitoring the voltage output of the piezoelectric sample through a high impedance probe (Fig. 6a).

As previously mentioned, the thickness of the piezoelectric transducer has to be adjusted in order to attain minimum necessary capacitance (*nF* order of magnitude) to ensure realistic impedance matching conditions. The dependence of clamped capacitance on the thickness of the lithium niobate layer with active surface area of 46 mm^2 is presented in Fig. 6b. The thickness of about 32 μm was selected for the experimentally studied structure as a trade-off between voltage magnitude, capacitance value, impedance matching conditions and structural (global) electromechanical coupling coefficient (*i.e.*, taking into account the Si layer). The clamped capacitance, C_0, of (YX*l*)/36° $LiNbO_3$ layer measured through an impedance analyzer was 0.79 nF (at 2 kHz), which was very close to the expected simulated value (0.83 nF). The frequency dependence of impedance modulus of the 32 μm thick piezoelectric (YX*l*)/36° $LiNbO_3$ crystal orientation in free conditions is presented in the inset of Fig. 6b. According to the equivalent lumped circuit, the structural coupling k_{eff}^2 of the structure was equal to 0.013. The *Q*–factor of the complete device, including the clamping system, estimated from the experimental data, was 23. This parameter can be improved changing the clamping system by means of thicker and heavier materials, which can lower the energy dissipation during the vibration cycles at the cost of size and weight.

The displacement and resonance frequency of the cantilevered (YX*l*)/36° $LiNbO_3$/Si beam tip were measured by means of an optical vibrometer (Polytec MSA-500). For this purpose, the beam was driven with a periodic, slowly varying chirp focused around the first resonance bending mode. The mechanical response of the cantilever as a function of frequency is given in Fig. 6c. The measured resonance frequency value f_0 was 1.14 kHz. Finite element simulations for this multilayer structure were also carried out, resulting in a first bending resonance mode at 1.16 kHz (Fig. 6c inset), in good agreement with the frequency found experimentally. The slight discrepancy was acceptable (5 % difference), and can be attributed to the perfect clamping conditions in simulation, fluctuations on the thickness value (± 2 μm) in the experimental apparatus and tolerance on the material elastic constants of both $LiNbO_3$ and Si.

After the characterization of the structure, we proceeded to test the device under constant excitation with the shaker, in order to investigate the piezoelectric harvesting possibility. In Fig. 7a are shown sinusoidal voltage and displacement signals measured under 3.4 g base acceleration at resonance frequency. The peak voltage amplitude obtained was $V_p = 21.1$ V, which corresponded to a tip displacement value of $u_p = 21.2$ μm, measured with the vibrometer. The root mean squared value of voltage at the resonance frequency was 14.9 V. After comparison with experimental data, FEM simulations results showed a slight overestimation of the voltage and displacement response. In fact, compared to the measured value, FEM overestimated the tip displacement by 3.3 μm. The simulated V_{rms} was approximately 15.8 V, giving a difference from the experimental value of 0.9 V. The reason behind the experimental and FEM values discrepancy (Table 2), is mostly due to a slight difference in terms of coupling and quality factors of the cantilever, as a result of using isotropic loss factor that was just an approximation of the real damping for the structure. This aspect can influence the displacement

magnitude and thus the voltage response. Eventually, from the measured values we could estimate the force factor α, defined as $\alpha = \frac{V_{pp}}{u_{pp}} C_0$, giving 0.882 mN.V^{-1}, and displacement magnitude u_M = 18.9 µm.

Finally, in order to validate the power that can be extracted from the (YXl)/36° $LiNbO_3$/Si beam driven by a monochromatic excitation at the vibration frequency f_0, a half-bridge circuit followed by a load, R_l, was connected to the piezoelectric material. The circuit is essentially composed by two 1N4148 diodes (Fast Switching Diode) and two smoothing capacitors, C_r, (each of 220 µF, resulting in an equivalent capacitor of 110 µF). Fig. 7b depicts the extracted experimental and theoretical (Eq. (7)) powers as function of load. The maximum power of 380 µW was attained experimentally for a 500 kΩ load impedance. Experimental results showed good agreement with the theoretical predictions (400 µW maximum power); although a slight difference can be noted probably due to some losses in the diodes (not taken into account in the theoretical model). According to the results, an experimental power density of 8.26 µW.mm^{-2} has been measured. This value is consistent with the best results for high-power piezoelectric generators (Table 3). It is important to note that the $LiNbO_3$/Si structures studied in this work were stiff and thus required high acceleration values in order to attain sufficient strain for high power densities. For the purpose of a fair comparison between our work and the state of the art, high frequency Si benders were taken into account. The table shows that even with normalized power density with respect to acceleration levels and frequency, the value of power of our device is comparable and even higher than other typical unimorph PZT and lead-free benders. In general, the power density is strongly correlated to the presence of a tip mass. For this reason, we adapted our finite element simulation to a smaller scale device in such configuration. The results for a micro mechanical transducer with silicon substrate are compared to the state of the art. The simulated device dimensions are 5 mm x 2 mm x 0.03 µm, with a tip mass of 250 µm, where the thickness of the piezoelectric film is reduced to 10 µm. The results show an instantaneous power output of 5.5 µW, that gives a very high normalized power density compared to other harvesters on silicon. Furthermore, with this simulation we can see how the presence of a proof mass lowers the resonance frequency while increasing the power density. Finally, as an application example, the piezoelectric material and its electrical harvesting interface have been connected to a custom sensor node (low-power Microchip PIC 16F15313 microcontroller driving an EnOcean PTM 330 node [26], V_{min} = 2.5 V – Fig. 8(a)). Fig 8(b) shows the voltage waveforms as well as the available energy on a 110 µF equivalent capacitor in such a configuration. As it can be deduced from Fig 8(b), the harvesting capabilities of the device allowed starting the sensor node (from zero energy initial conditions) after 9 seconds and then maintaining the possibility of sending data every 2 seconds (each transmission event consuming approximately 420 µJ) under continuous excitation.

6. Conclusion

This paper reported the implementation of $LiNbO_3$ layers as Pb–free piezoelectric transducers for a complete vibrational energy harvesting application. It was shown that commercially available (YX*l*)/36°

$LiNbO_3$ oriented wafers can be successfully implemented in the form of thick single-crystal films on Si substrate and effectively used by adjusting the thickness of the piezoelectric layer and consequently the capacitance, and by using a proper electronic configuration for energy harvesting. Results showed that the reported system yielded performances close to those of PZT materials. We would like to stress out that such performance of micro-transducers cannot be attained by using bulk $LiNbO_3$ wafers, due to impedance–matching issues. In fact, for bulk single crystals, the low value of the capacitance yields delicate interfacing with typical electrical circuit, while in this paper we are providing a more global approach towards energy harvesting applications. In terms of power density, experimental tests yielded 71 $\mu W.cm^{-2}.g^{-2}$ by using the proposed composite structure vibrating at resonance frequency of 1.14 kHz, that is among best values even compared to lead-based (and other lead-free) materials commercially available. Moreover, FEM simulations showed promising performances for MEMS scale devices based on $LiNbO_3$. Therefore, this result opens promising outcomes for lead-free energy harvesting solutions and their fast implementation. The fabrication of flexible structures based on thick $LiNbO_3$ layers will be considered in future to attain this efficiency at low frequency and acceleration values [4]. Although one finds some examples of high frequency resonating beams (Table 3), we will consider lowering the resonance frequency in order to match frequency spectra available abundantly in the environment, and design and fabricate bimorph structures to further increase the generated power. Concerning the coupling factors, we tailored the properties of the material in order to optimize the electro-mechanical coupling of the material, but future steps will also consider the optimization of the structural coupling in order to have maximum energy efficiency for our device.

Acknowledgments

This research was funded by European MSCN-ITN-ENHANCE program grant number 722496, French RENATECH network and EUR EIPHI program grant number ANR-17-EURE-0002.

List of Tables

Table 1. Comparison of dielectric and piezoelectric properties of (YXl)/36° $LiNbO_3$ with bulk materials.

Material	s_{jj}^E (pm².N^{-1})	s_{jj}^D (pm².N^{-1})	$\varepsilon_{ii}^T/\varepsilon_0$	d_{ij} (pC.N^{-1})	k_{ij}	FoM^T (10^{-12} m^3.J^{-1})	FoM^S (10^9 J.m^{-3})	Ref.
AlN	3.53	3.48	9.5	-2	0.12	0.048	3.87	[23]
KNN	8.2	7.6	496	-51	0.27	0.59	9.51	[24]
(YXl)/36° $LiNbO_3$	5.7	5.1	65.3	-18.1	0.32	0.57	19.5	[20]
PZT-5A	16.4	14.5	1700	-171	0.34	1.94	8.17	[21,22]
ZnO	7.87	7.59	11	-5.2	0.19	0.28	4.65	[25]

Table 2. Comparison of measured and simulated parameters for $LiNbO_3$ cantilever beam at 3.4 g.

Parameter	f_0 (Hz)	u_p (µm)	C_0 (nF)	V_{rms} (V)
Measured	1140	21.2	0.79	14.9
FEM	1163	24.5	0.83	15.8

Table 3. Comparison of piezoelectric high power density (PD) generators. The works selected represent the state of the art for high frequency silicon based devices. The power is normalized with respect to the active area, acceleration level and frequency.

Material	Tip Mass	Power (μW)	Area (mm^2)	$\vec{a}$ (g)	Frequency (Hz)	Areal PD ($\mu W/cm^2/g^2$)	Areal NPD ($10^{-2}\,\mu W/cm^2/g^2/Hz$)	Ref.
PZT	Yes	1.4	0.32	2	870	109	12.6	[27]
PZT	Yes	22	120	4	1300	1	0.09	[28]
PZT	No	3.4e-4	2.5	1	9275	0.014	1.5e-4	[29]
	Yes	13	2.5	1	2300	520	22.6	
KNN	No	1.1	56.1	1	1036	2	0.19	[30]
KNN	Yes	0.731	0.21	1.02	1509	335	22.2	[7]
ZnO	Yes	0.98	0.48	1.02	1300	196	15.1	[31]
AlN	Yes	0.8	0.32	2	1495	63	4.18	[32]
AlN	Yes	3.78	2.25	3	1041.4	19	1.79	[33]
AlN	Yes	34.78	27.3	2	572	32	5.57	[34]
AlN	No	0.003	3.21	0.4	4150	0.52	0.0126	[35]
	Yes	0.006	3.21	0.06	1140	52	4.56	
This work - (YXl)/36° $LiNbO_3$								
(*)	**No**	**380**	**46**	**3.4**	**1140**	**71**	**6.27**	**--**
(**)	**Yes**	**5.5**	**2**	**1**	**684**	**275**	**40.2**	**--**

(*) Experimental values for device without tip mass; (**) Simulated MEMS scale device with tip mass.

List of Figures

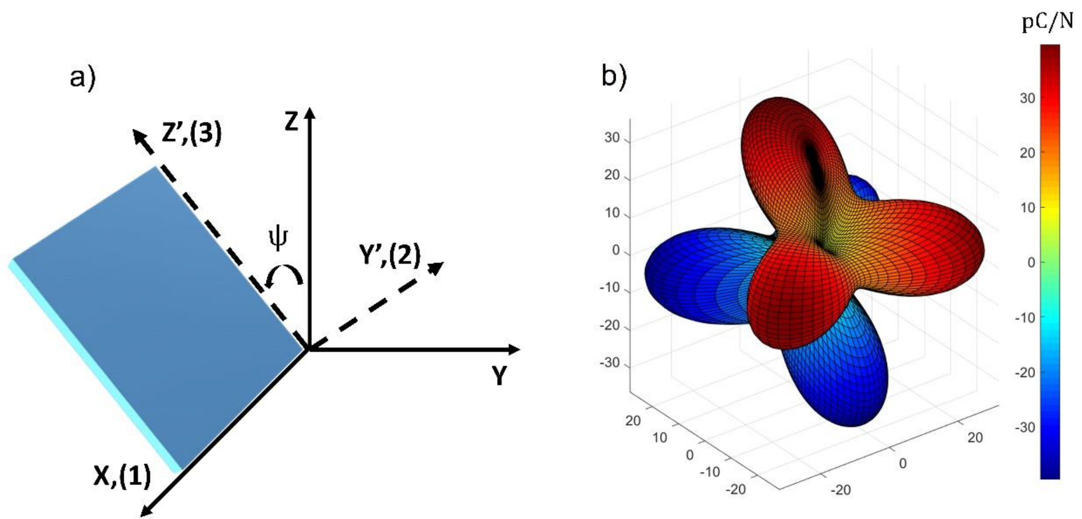

Fig. 1. (a) Reference system for simulation of (YXl)/36° $LiNbO_3$ orientation study. (b) Typical anisotropy of piezoelectric tensor of $LiNbO_3$ after rotation, both positive and negative values of the coupling are represented.

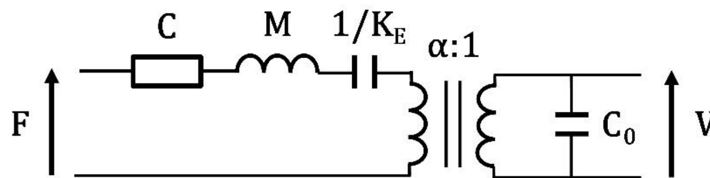

Fig. 2. Equivalent circuit for the piezoelectric transducer.

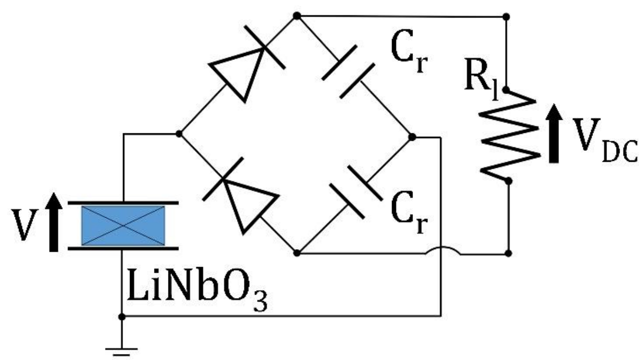

Fig. 3. $LiNbO_3$ generator connected to voltage doubler circuit and resistive load R_l.

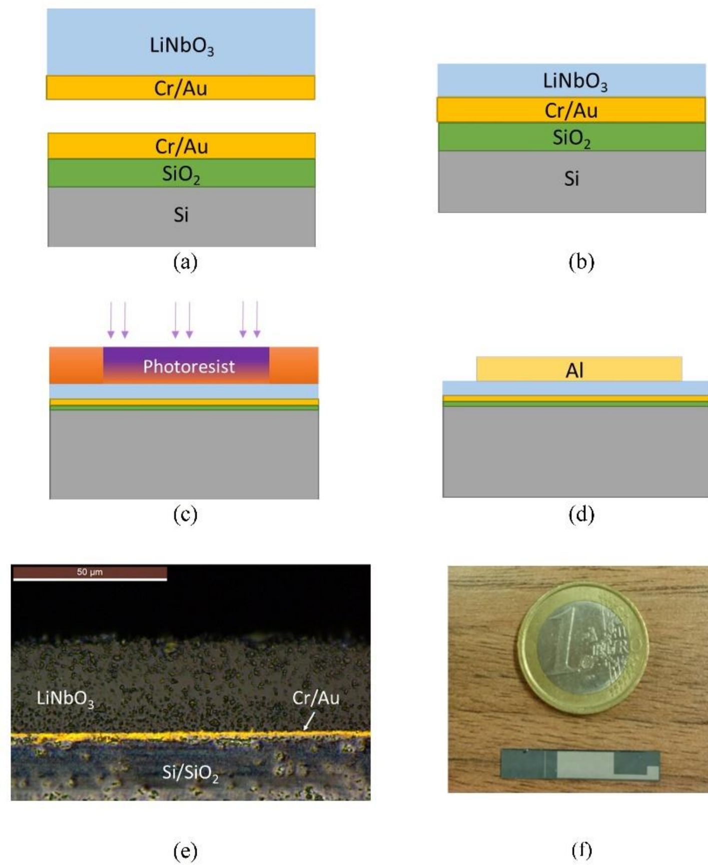

Fig. 4. Microfabrication process flowchart for (YXl)/36° $LiNbO_3$/Cr/Au/Cr/SiO_2/Si heterostructure: (a) 200 nm of Cr/Au were sputtered on the surface of both Si and $LiNbO_3$. (b) The two wafers were bonded together by mechanical compression and then thinned down by lapping. (c) The photoresist was spin-coated on the surface of $LiNbO_3$, and then exposed to UV light though a mask. (d) After evaporation of 300 nm of Al, the top electrode was patterned by lift-off. (e) Optical microscope cross-section photograph for the layer structure after dicing. (f) Eventually, the structures were mechanically diced in cantilever shape with an active surface of 46 mm².

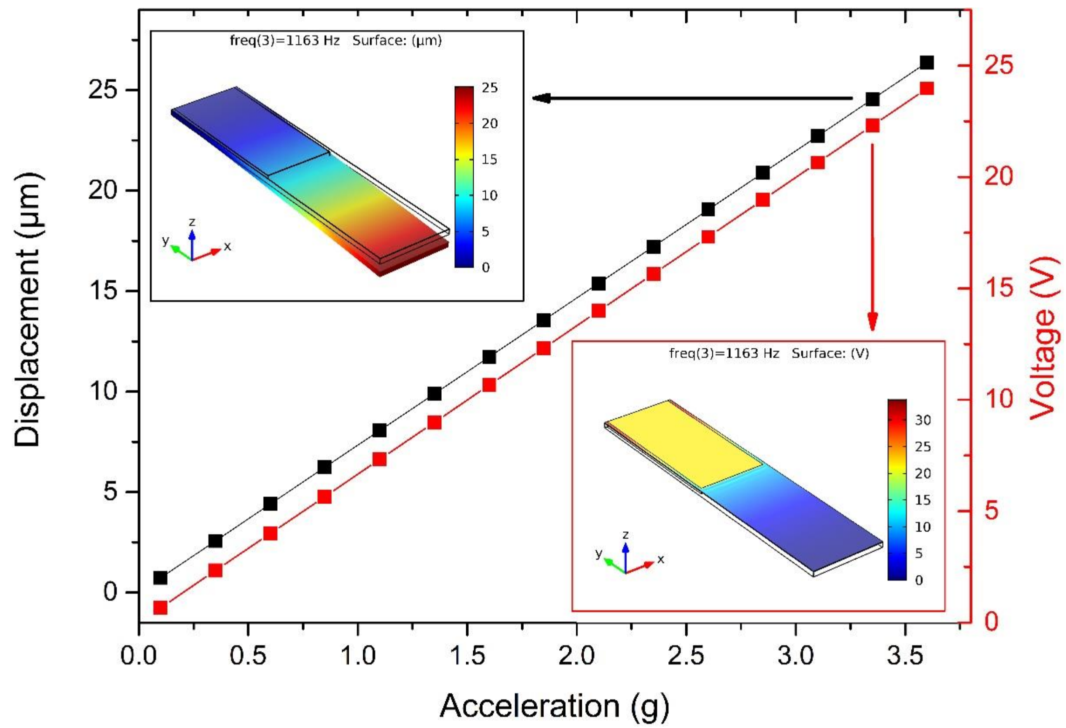

Fig. 5. Displacement and peak voltage results from FEM simulation at different acceleration levels. (insets) Deformation and voltage response of cantilever at resonance for 3.4 g.

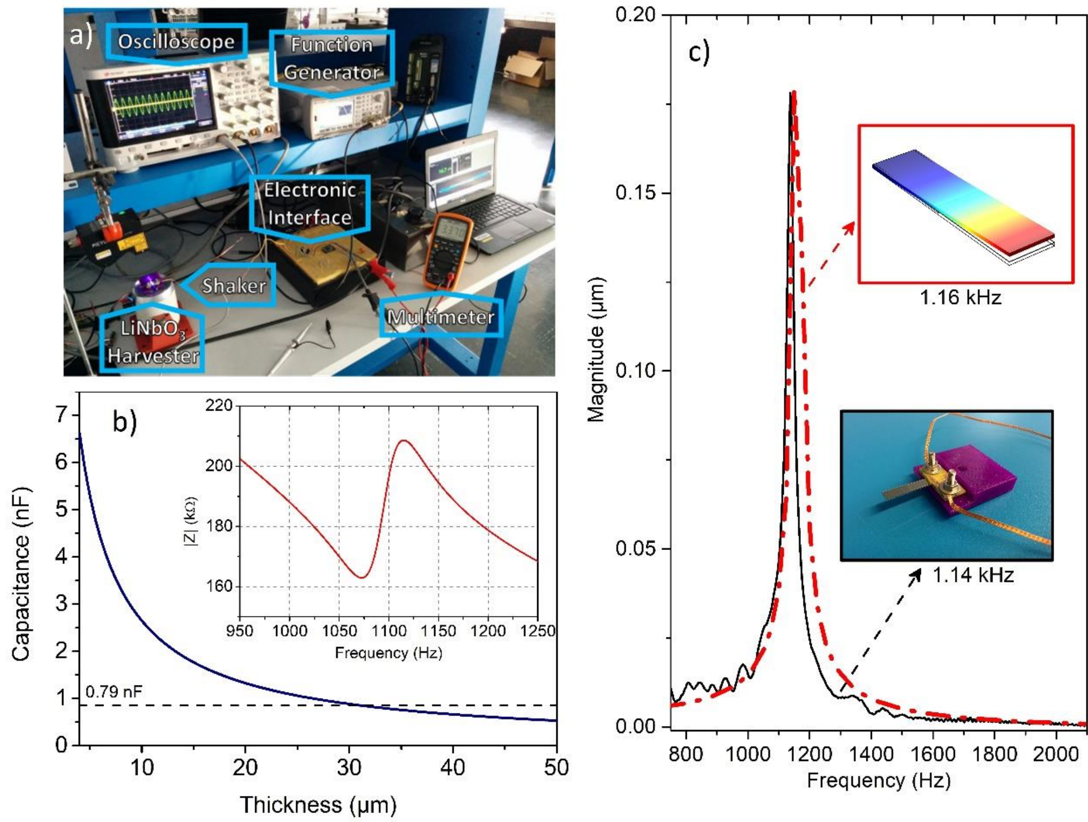

Fig. 6. (a) Photograph of setup for dynamic measurements testing. (b) Thickness dependence of parallel plate capacitor based on (YXl)/36° $LiNbO_3$ with active area of 46 mm^2 (b, inset) and frequency response of impedance modulus. (c) Displacement predicted by FEM simulation and measured experimentally by using optical vibrometer, of the studied (32 μm) (YXl)/36° $LiNbO_3$/Au/SiO_2/(360 μm)Si heterostructure. (c, inset) The simulated cantilever deformation (increases from blue to red) and the photograph of the experimentally fabricated transducer are given in the inset.

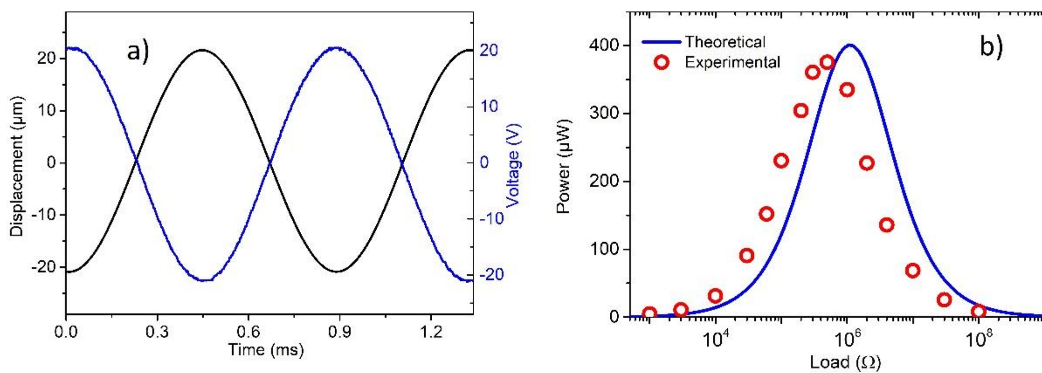

Fig. 7. (a) Displacement and generated voltage obtained through dynamic excitation with acceleration of 3.4 g. (b) Experimental and theoretical harvested power as a function of load by using (YXl)/36° $LiNbO_3$/Si harvester.

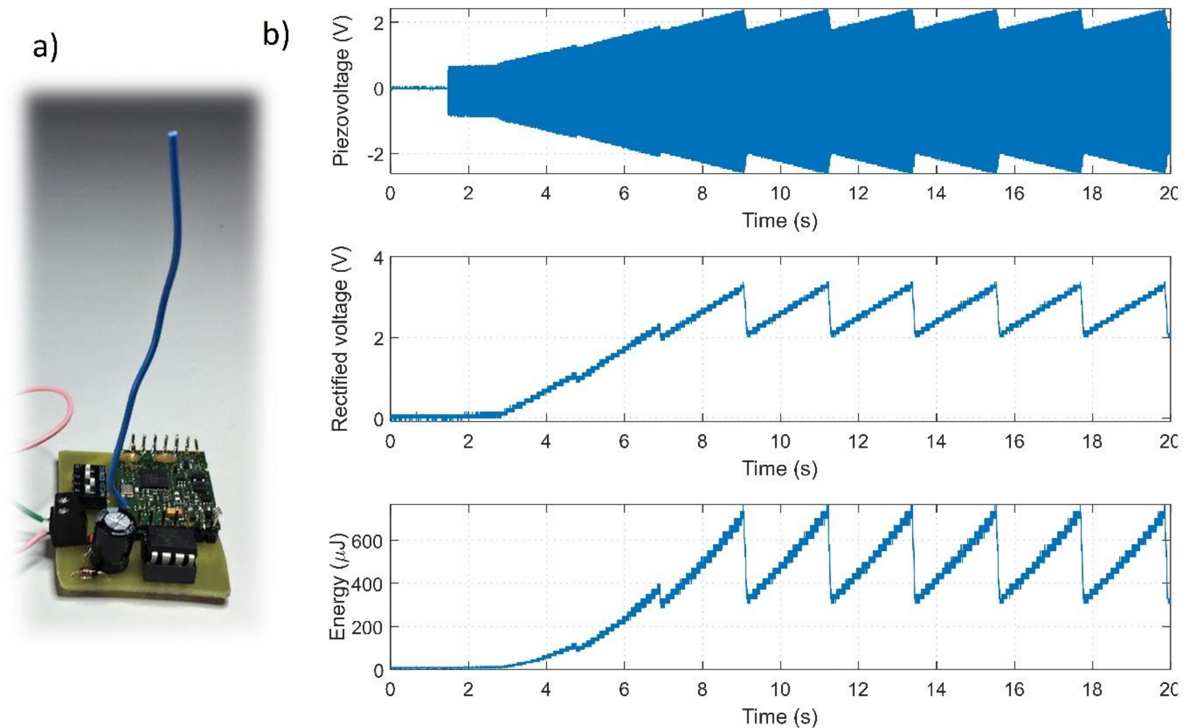

Fig. 8. (a) Photograph of sensor node featuring PIC 16F15313 micro-controller driving EnOcean PTM 330 RF Transmitter Module. (b) Experimental waveforms of piezoelectric transducer voltage, rectified voltage and available energy by using (YXl)/36° $LiNbO_3$ /Si harvester system (downswing in the waveforms correspond to transmission events).

References

[1] D. Spreeman and Y. Manoli, *Electromagnetic Vibration Energy Harvesting,* Springer (2012).

[2] S. P. Beeby, M. J. Tudor, and N. M. White, Energy harvesting vibration sources for microsystems applications, *Meas. Sci. Technol*. 17, R175 (2006).

[3] H. G. Yeo, T. Xue, S. Roundy, X. Ma, C. Rahn, and S. Trolier-McKinstry, Strongly (001) Oriented Bimorph PZT Film on Metal Foils Grown by rf-Sputtering for Wrist-Worn Piezoelectric Energy Harvesters, *Adv. Func. Mater*. 1801327 (2018).

[4] W. Tian, Z. Ling, W. Yu, and J. Shi, A Review of MEMS Scale Piezoelectric Energy Harvester, *Appl. Sciences 8*, 645 (2018).

[5] R. Matloub, M. Hadad, A. Mazzalai, N. Chidambaram, G. Moulard, C. S. Sandu, Th. Metzger, and P. Muralt, Piezoelectric Al1−xScxN thin films: A semiconductor compatible solution for mechanical energy harvesting and sensors, *Appl.Phys.Lett.* 102, 152903 (2013).

[6] M. Akiyama, K. Umeda, A. Honda, and T. Nagase, Influence of scandium concentration on power generation figure of merit of scandium aluminum nitride thin films, *Appl. Phys. Lett*. 102, 021915 (2013).

[7] L. Van Minh, M. Hara, and H. Kuwano, High Performance Nonlinear Micro Energy Harvester Integrated with (K, Na)NbO3/Si Composite Quad-Cantilever *IEEE Int. Conf. MEMS*, 397 (2014).

[8] J. Wu, D. Xiao, and J. Zhu, Potassium-sodium Niobate Lead-Free Piezoelectric Materials: Past, Present, and Future of Phase Boundaries, *Chem. Rev*. 115 (7), 2559 (2015).

[9] A. Bartasyte, S.Margueron, T. Baron, S. Oliveri, and P. Boulet, Toward High-Quality Epitaxial LiNbO3 and LiTaO3 Thin Films for Acoustic and Optical Applications, *Adv. Mater. Interfaces* **4** (8), 1600998 (2017).

[10] A. Baba, C. T. Searfass, and B. R. Tittmann, High temperature ultrasonic transducer up to 1000°C using lithium niobite single crystal, *Appl. Phys. Lett.* 97, 232901 (2010).

[11] E. D. Le Boulbar and C. R. Bowen, Study of Y-cut LiNbO3 (010) Crystal Under Oscillated Vibration at High Temperature for Energy Harvesting in Hostile Environment, *Joint IEEE ISAF, ISIF, PFM Proceed.* 292 (2015).

[12] T. Funasaka, M. Furuhata, Y. Hashimoto, and K. Nakamura, Piezoelectric Generator Using a LiNbO3 Plate with an Inverted Domain, *IEEE Ultrason. Symp. Proceed.* 1, 959 (1998).

[13] V. Bedekar, J. Oliver, S. Zhang, and S. Priya, Comparative Study of Energy Harvesting from High Temperature Piezoelectric Single Crystals, *Jpn. J. Appl. Phys*. 48, 091406 (2009).

[14] J. V. Vidal, A. V. Turutin, I. V. Kubasov, A. M. Kislyuk, M. D. Malinkovich, Y. N. Parkhomenko, S. P. Kobeleva, O. V. Pakhomov, N. A. Sobolev and A. L. Kholkin, Low-frequency vibration energy harvesting with bidomain LiNbO3 single crystals, *IEEE Trans. UFFC.* 66, 9 (2019).

[15] G. Kovacs, M. Anhorn, H.E. Engan, G. Visintini, and C.C.W. Ruppel, Improved material constants for LiNbO3 and LiTaO3, *Ultrason. Symp.* 435 (1990).

[16] A. H. Meitzler, D. Berlincourt, G. A. Coquin, F. S. Welsh III, H. F. Tiersten, and A. W. Warner, *IEEE Standard on Piezoelectricity*, ANSI/IEEE Std Series 176-1978, (1978).

[17] J.I. Roscow, H. Pearce, H. Khanbareh, S. Kar-Narayan and C. Bowen, Modified energy harvesting figures of merit for stress- and strain-driven piezoelectric systems. *Eur. Phys. J. Spec. Top.* 228, 1537-1554 (2019).

[18] T. Rödig, A. Schönecker, G. Gerlach, A Survey on Piezoelectric Ceramics for Generator Applications *J. Am. Ceram. Soc.* 93, 901 (2010).

[19] T. Baron, E. Lebrasseur, J.P. Romand, S. Alzuaga, S. Queste, G. Martin, D. Gachon, T. Laroche, J. Masson and S. Ballandras, Temperature compensated Radio-Frequency Harmonic Bulk Acoustic Resonators Pressure Sensors, *IEEE Int. Freq. Cont.* 652 – 655 (2010).

[20] A.W. Warner, M. Onoe, G.A. Coqin, Determination of Elastic and Piezoelectric Constants for Crystals in Class (3rn), *J. Acoust. Soc. Am.* 42 (6) 1223 (1966).

[21] A. Erturk and D. J. Inman, *Piezoelectric Energy Harvesting*, Wiley, (2011).

[22] Q. M. Zhang and J. Zhao, Electromechanical Properties of Lead Zirconate Titanate Piezoceramics Under the Influence of Mechanical Stresses, *IEEE Trans. UFFC* 46, 6 (1999).

[23] K. Tsubouchi, N. Mikoshiba, Zero temperature coefficients SAW devices on AlN epitaxial films, *IEEE Transactions UFFC*, vol. 32, n° 5, p. 634-644, (1985).

[24] A. Lenk, Elektromechanische Systeme, *Band 2 Systeme mit verteilten Parametern*, DK: 621.37.534, 2nd edition, VEB Verlag Technik, Berlin, (1977).

[25] H. Jaffe, and D. A. Berlincourt, Piezoelectric transducer materials, *Proceedings of the IEEE* 53 (10): 1372–1386, (1965).

[26] https://fr.farnell.com/b/enocean EnOcean PTM 330 – Radio Transmitter Module Datasheet (last viewed 16th December 2019).

[27] P. Muralt, M. Marzencki, B. Belgacem, F. Calame, S. Basrour, Vibration Energy Harvesting with PZT Micro Device *J. Am. Ceram. Soc.* 91, 1385–1396 (2009).

[28] A. Hajati, and S.-G. Kim, Ultra-wide bandwidth piezoelectric energy harvesting, *Applied Physics Letters* 99:083105, (2011).

[29] D. Isarakorn, D. Briand, P. Janphuang, A. Sambri, S. Gariglio, J.M. Triscoe, F.Guy, J.W. Reiner, C.H. Ahn, N.F. de Rooij, The realization and performance of vibration energy harvesting MEMS devices based on an epitaxial piezoelectric thin film, *Smart Mater. Struct.* 20, 025015 (2011).

[30] I. Kanno, T. Ichida, K. Adachi, H. Kotera, K. Shibata, and T. Mishima, Power-generation performance of lead-free (K,Na)NbO3 piezoelectric thin-film energy harvesters, *Sens. Actuator A-Phys.* 179:132–6 (2012).
[31] P. Wang, H. Du, ZnO thin film piezoelectric MEMS vibration energy harvesterswith two piezoelectric elements for higher output performance, *Rev. Sci.Instrum*. 86, 075002, (2015),.
[32] M. Marzencki, Y. Ammar, S. Basrour, Integrated power harvesting system including a MEMS generator and a power management circuit, *Sens. Actuator A-Phys.* 145–146, 363–370 (2008).
[33] J.Y. Zhang, Z.P. Cao, H. Kuwano, Fabrication of Low-Residual-Stress AlN Thin Films and Their Application to Microgenerators for Vibration Energy Harvesting, *Jpn. J. Appl. Phys.* 50, 09ND18 (2011).
[34] A.B. Alamin Dow, A. Bittner, U. Schmid, N.P. Kherani, Design, fabrication and testing of a piezoelectric energy microgenerator, *Microsyst. Technol.* 20,1035–1040, (2014).
[35] P.M. Mayrhofer, C. Rehlendt, M. Fischeneder, M. Kucera, E. Wistela, A. Bittner,U. Schmid, ScAlN MEMS cantilevers for vibrational energy harvesters purposes, *J. Microelectromech. Syst*. 26, 102–112, (2017).